JOURNAL OF MATERIALS SCIENCE **39** (2004) 5765–5770

Effect of rare-earth oxides on fracture properties of ceria ceramics

K. SATO
Fracture Research Institute, Graduate School of Engineering, Tohoku University, Aza-Aoba 01, Aramaki, Aoba-ku, Sendai 980-8579, Japan
E-mail: kazuhisa@rift.mech.tohoku.ac.jp

H. YUGAMI
Graduate School of Engineering, Tohoku University, Aza-Aoba 01, Aramaki, Aoba-ku, Sendai 980-8579, Japan

T. HASHIDA
Fracture Research Institute, Graduate School of Engineering, Tohoku University, Aza-Aoba 01, Aramaki, Aoba-ku, Sendai 980-8579, Japan

The influences of the sintering additive content of rare-earth oxide (Y_2O_3, Gd_2O_3, Sm_2O_3) on microstructure and mechanical properties of ceria ceramics were investigated by scanning electron microscopy and small specimen technique. A small punch testing method was employed to determine the elastic modulus and biaxial fracture stress of the ceria-based ceramics, and the fracture toughness was estimated by Vickers indentation method. Grain growth in the rare-earth oxides doped ceria ceramics was significantly suppressed, compared to the pure ceria ceramics. However, the elastic modulus, fracture stress and fracture toughness were decreased significantly with increasing additive content of the rare-earth oxides, possibly due to the oxygen vacancies induced by the rare earth oxides doping. The experimental results suggest that the change in the mechanical properties should be taken into account in the use of ceria-based ceramics for solid oxide fuel cells, in addition to the improvement of oxygen ion conductivity.

1. Introduction

Solid Oxide Fuel Cells (SOFCs) can generate high efficiency electric power using H_2 and O_2 gases without environmental pollution. Because SOFCs converts the chemical energy of the fuel directly to electrical energy without the intermediate of thermal energy, its conversion efficiency is not subject to the Carnot limitation. Because of their high temperature of operation (800–1000°C), natural gas fuel can be reformed within the cell stack eliminating the need for an expensive, external reformer system. Also, pressurized SOFCs can be successfully used as replacement for combustors in gas turbines; such hybrid SOFCs-gas turbine power systems are expected to reach efficiencies approaching 70% level. Thus, SOFCs are expected to become a major electric power source in the future [1, 2]. One of the traditional electrolyte materials are yttria-stabilised zirconia ceramics that must typically be operated at high temperatures, due to the relatively high resistivity of the electrolyte at lower temperatures. Lowering temperature, however, to between 600 and 800°C has a number of potential benefits, including, for example, cheaper materials, lower degradation problems, and closer temperature match for internal reformation possibilities. Ceria based ceramics, which have a higher oxygen ion conductivity than yttria-stabilized zirconia, is one of the possible electrolytes for SOFCs at low temperatures [3]. Many papers have been devoted to the study of rare-earth oxide additions on the electrical and the mechanical properties of ceria based ceramics [4–11]. However, in the previous studies the types and additive amount of rare-earth oxide investigated were limited and no systematic investigation has been undertaken so far. A small punch testing method was employed to conduct a systematic study using small sintered specimens. This paper presents experimental results of the systematic investigation on the effect of rare-earth oxides (Y_2O_3, Gd_2O_3 and Sm_2O_3) addition on the mechanical properties of doped ceria based ceramics.

2. Experimental

2.1. Sample preparation

Rare-earth oxide doped ceria powders with a composition of $(CeO_2)_{1-x}$ $(RO_{1.5})_x$(R = Y, Gd, Sm, x = 0, 0.10, 0.15, 0.20, 0.30, 0.40 and 1.0) were synthesized from CeO_2 (Anan Kasei Co. Ltd., Osaka, Japan, purity, 99.9%), Y_2O_3, Gd_2O_3 and Sm_2O_3 (Anan Kasei Co. Ltd., Osaka, Japan, purity, 99.9%) by a co-precipitation method. The powders were then pressed

into disks (ϕ12 × 1.0 mm) using a die press made of a hard metal at 50 MPa, followed by isostatic press at 120 MPa. The disks were then sintered in atmospheric condition at 1500°C for 5 h. Specimens were polished with Emery paper (#4000). After polishing, the specimens were annealed at 1000°C for 3 h to remove the induced residual stresses. The specimen densities of the sintered bodies were measured by the Archimedes method. The doped ceria ceramics with Y_2O_3, Gd_2O_3 and Sm_2O_3 are designated by YDC, GDC and SDC, respectively.

2.2. Experimental procedure

X-ray diffraction analysis of the sintered samples was conducted using a diffractometer (Mac science; M21Xmodel). The surfaces of specimens were thermally etched at 1400°C. In order to observe the microstructure of the sintered bodies and measure the grain size, the specimens were examined using scanning electron microscopy (SEM).

The mechanical properties of the sintered bodies, the Young's modulus and fracture stress were measured by a small punch (SP) testing method [12] using miniaturized disk specimens. The punch and specimen holder, designed for SP tests, are shown in Fig. 1. The SP tests were performed on a universal testing machine (Instron 1185 type) in atmospheric condition at room temperature. The diameter and thickness of specimens were ϕ10, and 0.7 mm, respectively. The specimen holder consists of an upper and lower die. The load application was performed through the puncher until a final failure occurred at a crosshead speed of 0.1 mm/min. The deflections of the specimens were measured by monitoring the movement of an Al_2O_3 rod using a linear variable differential transducer (LVDT) fixed on to the Instron machine. The resolution of the LVDT used in this study was within 0.1 μm.

Deformation and stress analysis for SP tests have been performed using a finite element method (FEM), assuming linear elastic response of the material [12]. In this study, the numerical data were used to compute the Young's modulus and fracture stress. The Young's modulus and biaxial tensile stress of SP specimens can be expressed by the following equations [13]

$$E_{SP} = f(t/a)\frac{3a^2P(1-\nu)(3+\nu)}{4\delta\pi t^3} \quad (1)$$

$$\sigma_{SP} = \frac{P}{t^2}(1+\nu) \times \left[0.485\ln\frac{a}{t} + 0.52 + \frac{3}{2\pi(1+\nu)}\right] \quad (2)$$

where P is the load, δ the deflection at the specimen center, ν the Poisson's ratio, t the specimen thickness (= 0.7 mm), a the bore diameter of the lower die (=2.38 mm) and $f(a/t)$ the correction factor for specimen thickness (=1.13). The value of Poisson's ratio was assumed to be 0.33, following the reported data for doped ceria ceramics [8]. The Young's modulus was calculated from the initial linear slope of the load-deflection curve using Equation 1. The fracture stress was calculated from the maximum load using Equation 2. The Young's modulus and fracture stress were determined from the SP method is referred to as E_{SP} and σ_{SP}, respectively. Four or five specimens were tested for each dopant content. Indentation was performed on the polished dry-surface of the sample, using an Akashi MVK-E type Hardness Tester with a standard Vickers indenter. The indenter load was kept at 9.8 N for 15 s. Three to five measurements were performed on each specimen. The fracture toughness, K_c can be calculated using the following equation (JIS R 1607)

$$K_c = 0.018\left(\frac{E}{HV}\right)^{\frac{1}{2}}\left(\frac{P}{C^{\frac{3}{2}}}\right) \quad (3)$$

where E is the Young's modulus, HV the Vickers hardness, P the applied indenter load (9.8 N) and C the surface radial crack length.

3. Results and discussion

3.1. Microstructure of doped ceria ceramics

The relative density of the doped ceria ceramics sintered at 1500°C was shown to be 99 ± 0.2% for YDC, GDC, and SDC. Fig. 2 shows an example of XRD pattern for a sintered specimen of 10YDC, along with the diffraction peak angles of pure ceria ceramics. The

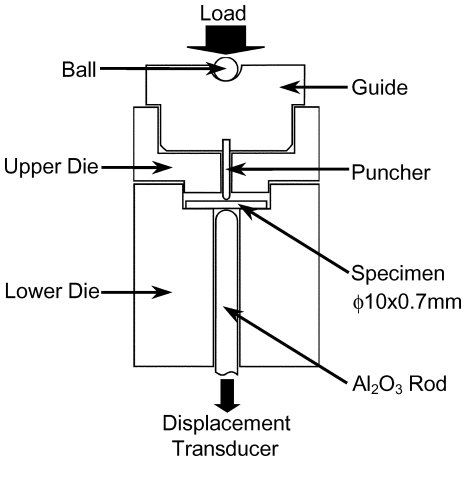

Figure 1 Schematic illustration of small punch testing method.

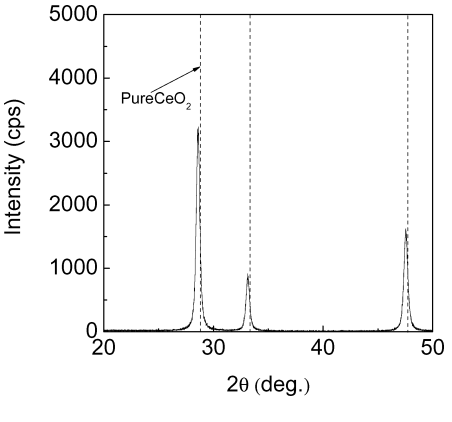

Figure 2 X-ray diffraction pattern of YDC ($(CeO_2)_{0.9}(YO_{1.5})_{0.1}$).

sintered 10YDC shows the XRD pattern of cubic ceria with a shift to slightly lower diffraction angles. This observation indicates that the solid solution of 10YDC has been produced by the processing conditions employed in this study. All the doped ceria ceramics prepared in this study were observed to show a XRD pattern similar to the 10YDC, irrespective of the different dopants. Fig. 3a–d show SEM photographs of the microstructure for 0, 10, 40 and 100 mol% Sm_2O_3 doped ceria ceramics, respectively. The observations have been made using thermally etched specimens. The grain shape of all samples is either regular pentagon or hexagon, whereas the pure Sm_2O_3 exhibits an inhomogeneous structure with elongated grains surrounded by finer ones (Fig. 3d). It is also seen that the addition of the dopant significantly influences the grain size of the sintered ceramics. The effect of Y_2O_3, Gd_2O_3 and Sm_2O_3 on the average grain size is shown in Fig. 4. The average grain size was determined by measuring the mean intercept length of test lines using SEM photographs. The average grain size for the pure Y_2O_3 and Sm_2O_3 ceramics is also indicated in Fig. 4. No fully sintered body

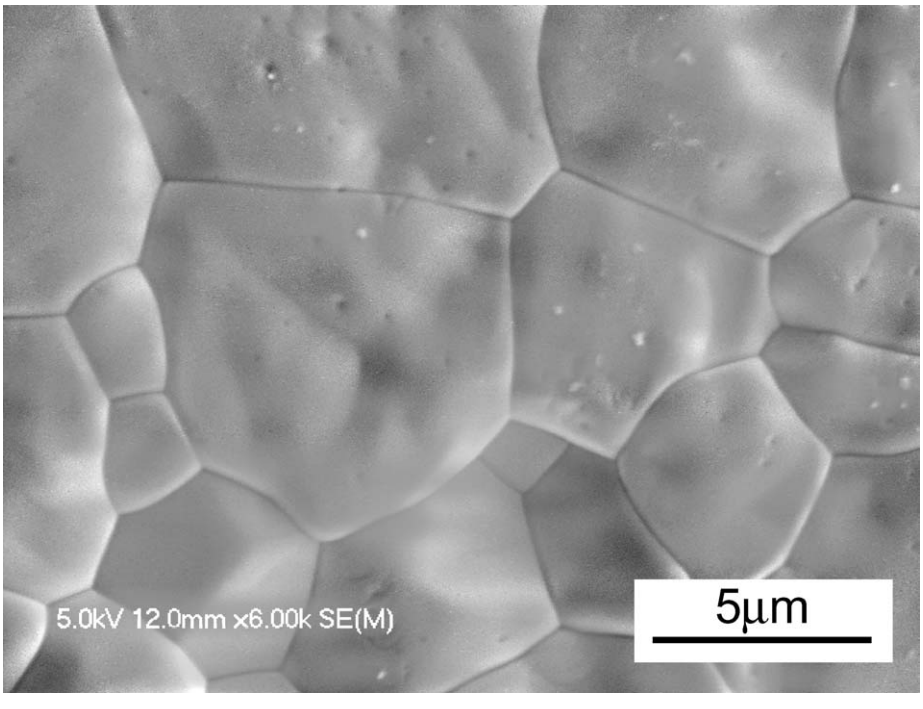

(a)

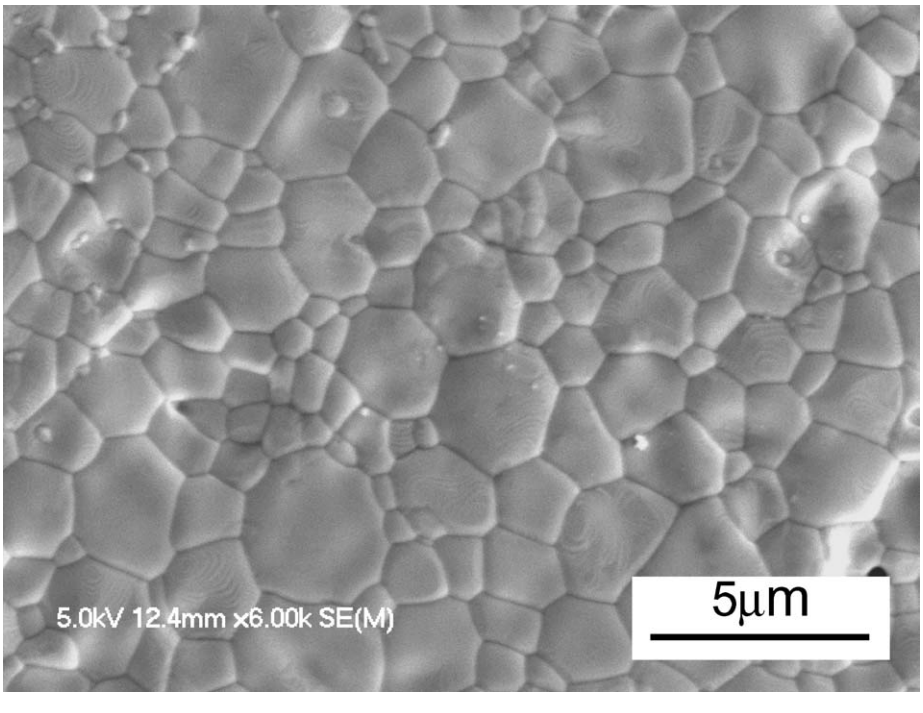

(b)

Figure 3 Scanning electron micrographs of microstructure of doped ceria ceramics (SDC). (a) Pure CeO_2, (b) 10 mol% Sm_2O_3-CeO_2, (c) 40 mol% Sm_2O_3-CeO_2 and (d) Pure Sm_2O_3. (*Continued*)

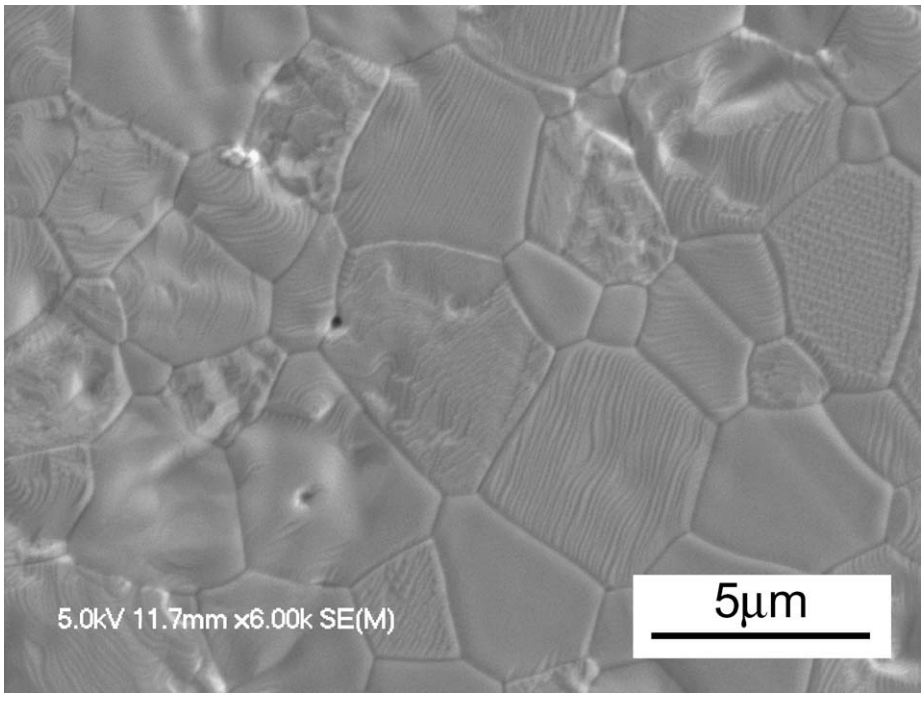

(c)

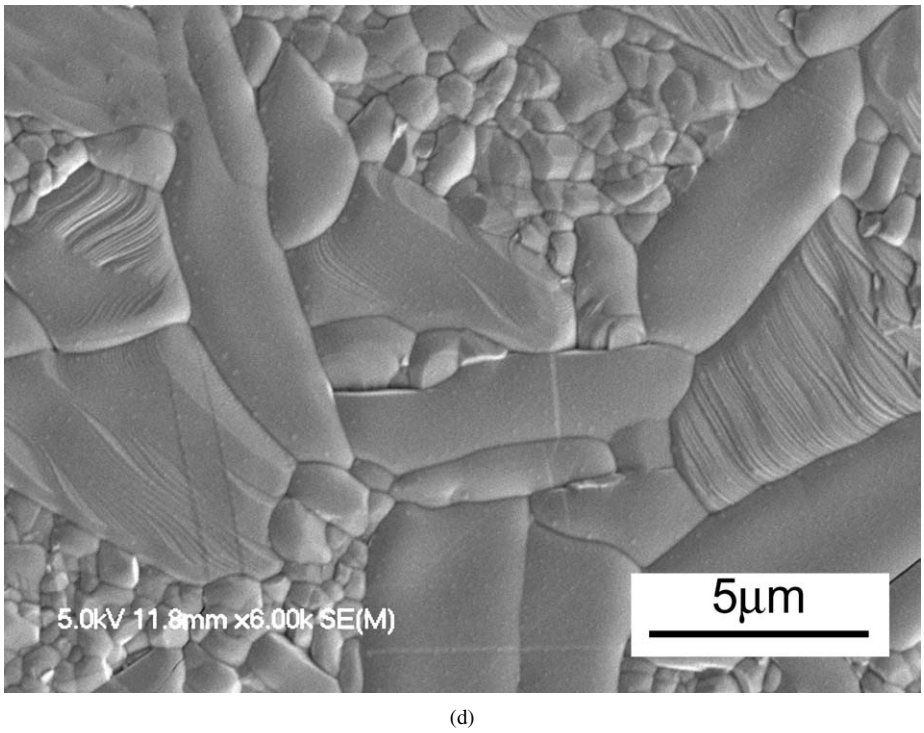

(d)

Figure 3 (*Continued*)

was achieved for pure Gd_2O_3 and only a porous body was prepared at 1500°C in this study (the relative density was 60%). It appears that the relationship between the grain size and the dopant content is insensitive to the dopant type used. The grain size is shown to initially decrease from the value of the pure ceria ceramics (4.1 μm), and show a minimum value at the dopant content of 10–20 mol%, regardless of the dopant type.

The color of the doped ceria ceramics was shown to depend on the dopant content and changed from brown to yellow and finally white color as the dopant content was increased. It is well known that the color of doped ceria ceramics is generally sensitive to the valence of the ceria. The cause of the color change may be due to the change in valence.

3.2. Deformation and fracture properties

Examples of the load vs. deflection relationship obtained from the SP tests are shown in Fig. 5. All specimens show a linear elastic fracture behavior, except for the pure Sm_2O_3. The arrow indicates the deflection at which the catastrophic fracture took place. The pure Sm_2O_3 exhibits a quasi-brittle fracture after the peak stress, characterized by the serrated load vs. deflection curve. The quasi-brittle fracture behavior in the pure

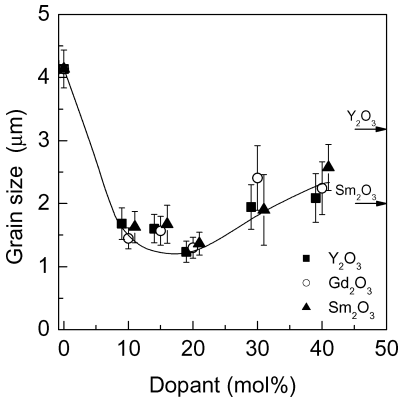

Figure 4 Grain size of $(CeO_2)_{1-x}(RO_{1.5})_x$ as a function of the dopant content.

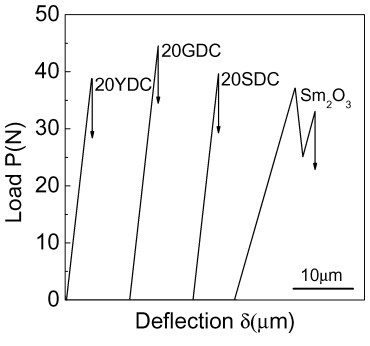

Figure 5 Load versus deflection curves.

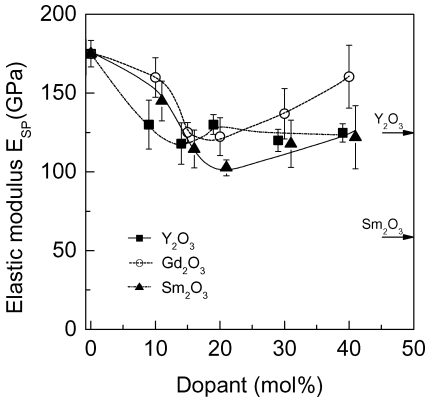

Figure 6 Young's modulus E_{SP} of $(CeO_2)_{1-x}(RO_{1.5})_x$ as a function of the dopant content.

Sm_2O_3 may be due to the formation of the elongated grains as observed in Fig. 3d. The elongated grains with high aspect ratio are expected to contribute in trapping and bridging the propagating crack.

The Young's modulus E_{SP} of the doped ceria ceramics is plotted as a function of the dopant content in Fig. 6. All the doped ceria ceramics have lower Young's modulus values than that of the pure ceria within the range of the dopant content used in this study. In the case of the YDC, E_{SP} appears to decrease as the dopant content is increased and give a minimum value at the dopant content of 15 mol%. The GDC and SDC show a similar trend and give a minimum E_{SP} value at the dopant content of 20 mol%. Fig. 7 summarizes the fracture strength of the doped ceria ceramics determined using the SP method. It is seen that the variation of

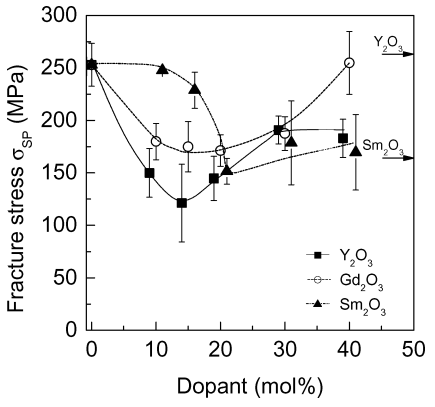

Figure 7 Fracture stress σ_{SP} of $(CeO_2)_{1-x}(RO_{1.5})_x$ as a function of the dopant content.

the fracture strength with the dopant content is approximately similar to that of the Young's modulus. Thus, the strength reduction induced by the doping may be due to the increased concentration of oxygen vacancies. Fracture strength usually increases with the decreasing grain size. However, as shown in Figs 4 and 7, the fracture strength shows a minimum value approximately for the range of the smallest grain size (10–20 mol% dopant). It appears that the influence of the increased oxgen vacancies override strengthening effect due to the finer grain size.

The fracture toughness K_c measured using the indentation method is plotted in Fig. 8 as a function of the dopant content. The fracture toughness value is observed to decrease monotonically as the dopant content is increased, even though 10GDC and 10SDC give approximately the same fracture toughness value as that of the pure ceria. After the indentation tests, the specimen were thermally etched at 1400°C to reveal the grain boundaries at surface. The lengths of transgranular fractures were measured along the four radial cracks induced by the indentation for each specimen. The total length of the transgranular fractures were divided by the entire length of the indentation cracks to determine the ratio of transgranular fracture for each specimen. Fig. 9 shows the ratio of transgranular fracture determined from the indentation tests. It can be seen that the transgranular fracture ratio in the doped ceria ceramics increases with the increasing dopant content, reflecting

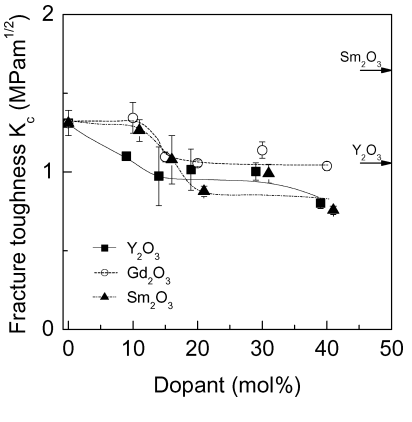

Figure 8 Fracture toughness K_c of $(CeO_2)_{1-x}(RO_{1.5})_x$ as a function of the dopant content.

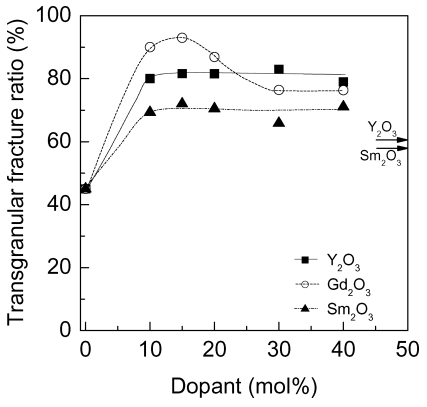

Figure 9 Transgranular fracture ratio of $(CeO_2)_{1-x}(RO_{1.5})_x$ as a function of the dopant content.

probably the reduced grain strength due to the increased concentration of oxygen vacancies.

The above-mentioned experimental results suggest that the change in the mechanical properties should be taken into account in the use of the ceria-based ceramics for solid oxide fuel cells, in addition to the improvement of oxygen ion conductivity.

4. Conclusions

The main results obtained from this study can be summarized as follows:

1. The grain size of the doped ceria ceramics was shown to initially decrease as the increasing dopant content and then increase with the further addition of the dopant. A minimum value grain size was produced at the dopant content of approximately 10–20 mol%, regardless of the dopant type.

2. The Young's modulus and fracture stress of the doped ceria ceramics determined by a small punch testing method were lower than that of a pure ceria within the range of the dopant content used in this study. Especially, the mechanical properties gave a minimum value at the dopant content of 10–20 mol%, possibly to due the increased oxygen ion vacancies in the doped ceria ceramics.

The fracture toughness value obtained by Vickers indentation method was observed to decrease monotonically as the dopant content is increased.

3. The transgranular fracture ratio in the doped ceria ceramics increased with the increasing dopant content, reflecting probably the reduced grain strength due to the increased concentration of oxygen vacancies.

Acknowledgements

The authors would like to thank Anan Kasei Co., Ltd. for supplying the powders of ceria ceramics.

References

1. N. Q. MINH, *J. Amer. Ceram. Soc.* **76** (1993) 563.
2. S. C. SINGHAL, *Solid State Ion.* **135** (2000) 305.
3. H. INABA and H. TAGAWA, *ibid.* **83** (1996) 1.
4. M. MOGENSEN, N. M. SAMMES and G. A. TOMPSETT, *ibid.* **129** (2000) 63.
5. H. YAHIRO, K. EGUCHI and H. ARAI, *ibid.* **36** (1989) 71.
6. C. TIAN and S.-W. CHAN, *ibid.* **134** (2000) 89.
7. S. SAMESHIMA, T. ICHIKAWA, M. KAWAMINAMI and Y. HIRATA, *Mater. Chem. Phys.* **61** (1999) 31.
8. A. ATKINSON and A. SELCUK, *Solid State Ion.* **134** (2000) 59.
9. N. SAMMES, G. TOMPSETT, Y. ZHANG, A. CARTNER and R. TORRENS, *Denki Kagaku* **64** (1996) 674.
10. J. VAN HERLE, R. IHRINGER, N. M. SAMMES, K. KENDALL, K. YAMADA, C. WEN, T. KAWADA, M. IHARA and J. MIZUSAKI, *Solid State Ion.* **132** (2000) 333.
11. O. BELLON, N. M. SAMMES and J. STANIFORTH, *J. Power Sources* **75** (1998) 116.
12. Y.-H. JOO, T. HASHIDA, H. TAKAHASHI and K. SHIMOMURA, *J. Test. Eval.* **20** (1992) 336.
13. S. OKUDA, M. SAITO, T. HASHIDA and H. TAKAHASHI, *Trans. JSME(A)* **57**(536) (1991) 940.

Received 22 July 2003
and accepted 9 March 2004